Int. J. Electrochem. Sci., 17 **(2022)** Article Number: 220116, doi: 10.20964/2022.01.16

International Journal of
ELECTROCHEMICAL
SCIENCE
www.electrochemsci.org

Effect of the Geometric Parameters of the Rib-Channel and Porous Cathode on the Species Distribution in the Cathodes of Protonic Ceramic Fuel Cell Stack

Jiaqi Dai[1], *Delphine Uwaneza*[1], *Aleksey Levtsev*[2], *Zidong Yu*[1], *Daifen Chen*[1,*]

[1] School of Energy and Power Engineering, Jiangsu University of Science and Technology, Zhenjiang 212100, China
[2] National Research Ogarev Mordovia State University, Saransk 430005, Russia
[*]E-mail: dfchen01@163.com

Received: 30 September 2021 / *Accepted:* 29 October 2021 / *Published:* 6 December 2021

Proton ceramic fuel cell (PCFC) has attracted more and more attentions because of its advantages in the intermediate temperature operation zone. In this paper, a typical 5-cells PCFC stack is established and can be used for three-dimensional calculated fluid dynamics (CFD) model. Then the effects of different configurations and geometric parameters on species distributing qualities within the cathode components are studied and discussed. The result shows that increasing the width of the rib channel and the thickness of the porous cathode can greatly enhancing the oxygen supplying and vapor removing capabilities, especially for those electrochemical reaction sites covered by the solid ribs. In order to improve the electrochemical reaction, a more practical cathode bipolar plate structure with PCFC should be further developed.

Keywords: Protonic ceramic fuel cell, Oxygen supplying and vapor removing capabilities, 3D calculated fluid dynamics, Structure and performance.

1. INTRODUCTION

The use of fuel and the combustion of fossil energy are greatly increased all over the world. Limited by Carnot cycle, traditional thermal power generation technology cannot make good use of fuel energy in current technology art [1, 2]. Efficient and renewable new energy has become the focus of current research [3]. Fuel cells which can directly convert chemical energy into electrical energy have been widely studied [4-9]. There are many kinds of fuel cells, which are generally classified according to different electrolytes. Solid oxide fuel cell is one of the most famous type that uses the solid ionic conductive ceramic materials It consists of both the oxygen conducting solid oxide fuel cell (O^{2-}-SOFC) that is operated around the high temperature zone (600-1000^{o}C) and the protonic ceramic fuel cell (PCFC) that is operated around the intermediate temperature zone (400-700^{o}C) [10-13],

This is because compared with the activation energy required for conducting oxygen ions (0.80 eV), the activation energy required for conducting protons (0.3-0.6 eV) is greatly reduced [14], PCFC can be operated at the intermediate temperatures and use more hydrocarbons as fuels [15-17]. Compared with PEMFC, PCFC can use cheaper oxides as catalysts [18]. It is more superior in economic performance or service conditions [19]. Recently, more and more studies for the composite cathode and anode materials of PCFC have being taken place to further improve its ionic and electronic conducting performances [9, 20]. The structural design and optimization of the stack and the corresponding components are generally considered to be the important factors affecting the performance of fuel cells [21, 22]. These will further affect the electrochemical reactions and multi-physical coupling processes in the fuel cells [23, 24].

K. Ding et al. established a five layer fuel cell model and studied its internal component distribution, temperature and current distribution details [25]. The flow distribution and pressure drop of various PEMFCs with different channel structures were compared by modeling and the optimized air flow channel was obtained [26]. As far as we know, the research on both SOFC and PEMFC has been very mature, but the research on PCFC is just started. There are many aspects worthy of research, such as more durable metal parts, electrolytes with higher conductivity and more suitable components and stack structures [11, 27]. D. Chen et al. established a 20 layer fuel cell model based on both counter and co-flows to study the uniformity of air and fuel distribution within the stack [28]. Changing the structure and geometric parameters of the rib channels, such as the configuration of the header, will affect the distribution of the fuel and oxygen distribution qualities over the electrolyte surface. Yu Xu et al. established a physical model of single cell SOFC, which combined with momentum, component and energy conservation equations, and predicted the dependence of the species distributing qualities on the flow path structure and parameters [5]. Obviously, PCFCs do not perform at their best, partly because of their different cathode products compared with the ordinary SOFC. However, there is no cathode configuration specially designed for PCFC [29].

In this paper, three-dimensional calculated fluid dynamics will be used to study the effects of different configurations and geometric parameters on a typical PCFC stack with 5-cells, such as, the rib shape, width, thickness of cathode layer and so on, on species distributing qualities within the cathode components. It plays a certain role in the technical progress and development of PCFC stack, and the appropriate stack design is obtained.

2. STACK CONFIGURATION AND CALCULATION FLUID MODEL

In **Fig. 1** a typical fuel cell stack structure for PCFC is displayed. MEA unit is composed of anode support layer, anode functional layer, dense electrolyte, cathode functional layer and cathode current collect layer. The bipolar plates are connected in series to prevent the excess output electric current and improve the operation output voltage of the stack. One side of the bipolar plate is the cathode rib channel and the other side is the anode channel. Air and fuel will be spread over the cathode and anode surfaces by the cathode and anode rib channels, respectively. The inlet and outlet manifold and header are also placed on the bipolar plate to transport fuel and air to each layer of stack. The manifold used in this paper

is distributed into two inlet manifolds on the left and three outlet manifolds on the right. The electrochemical reaction of the cathode in PCFC stack is directly related to the air flow path and oxygen diffusion path. The 3D CFD model for cathode part of the stack will be developed to study the relationship between the flow path configuration on the air and oxygen distribution.

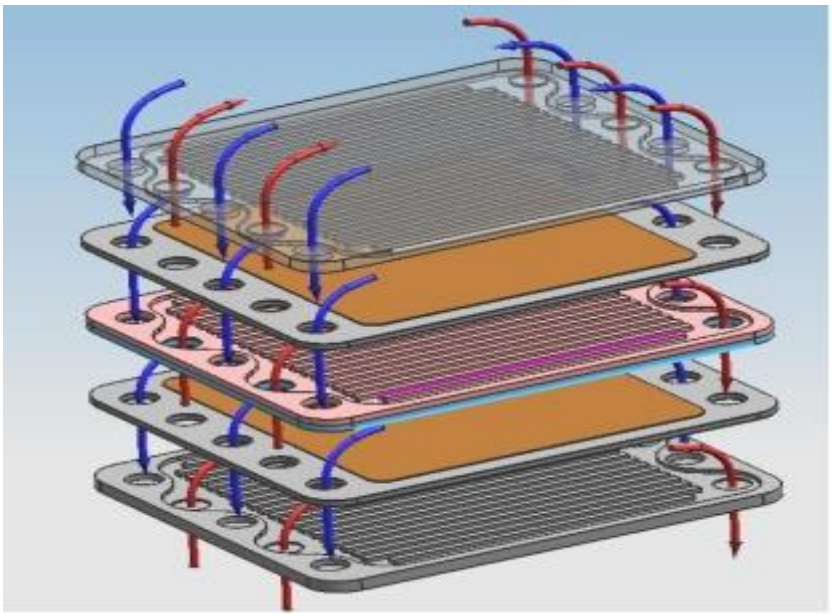

Figure 1. A typical planar fuel cell structure for a PCFC stack.

Fig. 2 More in-depth shows the component of the air and oxygen transport paths within a single layer of PCFC stack. Geometric parameters related to stack are described in **Table. 1**. The 3D model will include: i) two air inlet manifolds; ii) three air outlet manifolds; iii) rib channels and feed/exhaust headers; iv) cathode support layer (CSL); cathode functional layer (CFL).

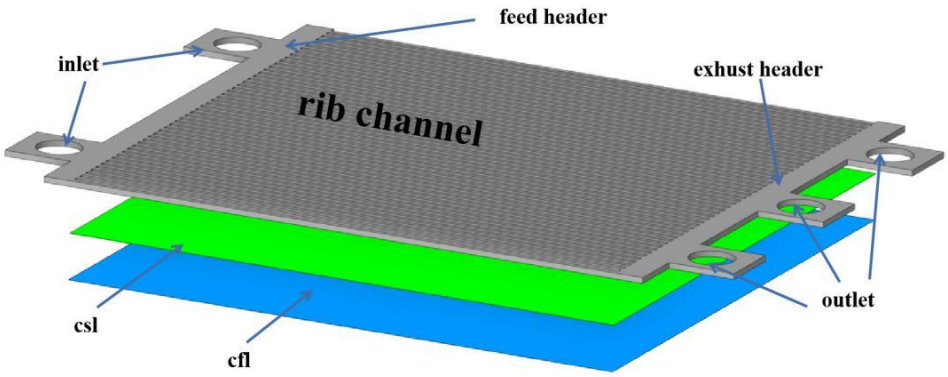

Figure 2. Schematic diagram of rib channel and electrode of single layer.

Table 1. Configuration parameters of stack and single-layer model size.

Parameters	Geometric sizes
MEA area	100×100 mm²
The thickness of cathode support layer	0.05 mm
The thickness *l* of cathode function layer	0.01, 0.02 and 0.03 mm
Solid ribs (x,y,z)	100 mm × 2 mm × 1 mm
Rib channels (x,y,z) w_{rc}	100 mm × 2 mm × 1 mm
Radius of air inlet manifold r_{in}	4 mm
Radius of air outlet manifold r_{out}	4 mm
Operating temperature of PCFC	473 K
Output current density i_{op}	5000 A·m^{-2}
The oxygen utilization	0.2

The CFD governing equation is applicable to the 3D 5-cells PCFC stack model. Using the continuity equation and momentum conservation equation, the flow distribution in the inlet/outlet manifold and cathode rib channel can be calculated,

$$\nabla\cdot\left(\rho\boldsymbol{u}\right)=0 \tag{1}$$

$$\nabla\cdot\left(\rho\boldsymbol{u}\times\boldsymbol{u}\right)=-\nabla P+\rho\boldsymbol{f}+\mu\left(\frac{1}{3}\nabla\left(\nabla\cdot\boldsymbol{u}\right)+\Delta\boldsymbol{u}\right) \tag{2}$$

where ρ, $\boldsymbol{u}$, P are the density, velocity vector and static pressure of the fluid, respectively. μ is the effective dynamic viscosity, which is calculated by the ideal air mixing law,

$$\mu=\sum_{\alpha=1}^{n}\frac{\chi_\alpha\mu_\alpha}{\sum_{\beta=1}^{n}\chi_\beta\Phi_{\alpha,\beta}} \tag{3}$$

Below the operation temperature *T*, the value of μ_α can be calculated using Sutherland's law,

$$\frac{\mu_\alpha}{\mu_\alpha^0}\approx\left(\frac{T}{T_0}\right)^{1.5}\frac{T_0+S}{T+S} \tag{4}$$

where *S* is the Sutherland constant.

The diffusion of species in porous cathode and functional layer can be calculated by formula,

$$\nabla\cdot\left(\varepsilon\rho Y_\alpha\boldsymbol{u}\right)=\nabla\cdot\left(\rho D_{\alpha,eff}\nabla Y_\alpha\right)+S_\alpha \tag{5}$$

where ε is the porosity of the porous mediums. Y_α and $D_{\alpha,\text{eff}}$ are the mass fraction and effective diffusion coefficient of species α, S_α is the species source item. The source term of PCFC stack cathode function layer can be expressed as,

$$S_{O_2}=-\frac{i_{op}M_{O_2}}{4Fl},\quad S_{H_2O}=\frac{i_{op}M_{H_2O}}{2Fl},\quad S_{N_2}=0 \tag{6}$$

The value of *l* represents the thickness of the cathode functional layer. M_α is the molar mass of species α. *F* is the Faraday constant. Electrochemical reactions generally occur on the surface of electrolyte [30]. The hypothesis was proved to be reasonable and its impact on the results was negligible [31].

In the airflow path of the stack, the air flows from the inlet to the outlet and is discharged through the outlet manifold. The air flow inside the path and on the electrolyte surface is continuous. The boundary part is adiabatic and does not slip. The *k-epsilon* is the value used in the three-dimensional calculation of turbulence model, and the boundary conditions are set as velocity inlet and pressure outlet. The average current density i_{op} determines the flow rate at the inlet, stack layer number *N*, the active surface area is *A* , which determines the oxygen utilization η_{O_2} .

$$u_{\text{air}}^{\text{in}} = \frac{Ni_{\text{op}}AM_{air}}{4F\eta_{O_2}\chi_{O_2}\rho_{air}A_{air}} \quad (7)$$

where χ_{O_2} is the mole fraction of oxygen in the inlet feeding air flow. A_{air} is the cross-sectional area of the total air entrances.

3. RESULT AND DISCUSSION

Figs. 3a and **b** shows the oxygen distributions within the 5-cells PCFC stack and over the dense electrolyte surface, while the width of the rib channel w_{rc}=2 mm and i_{op}= 5000 A m^2. From the figures, it is found that the width of the rib channel has a great impression on the oxygen transportation in the air flow path. Compared with the calculated results reported by the previous paper [13], we can get that the air flow feeding conditions among the rib channels will determine the corresponding oxygen distribution quality. This will further affect the species distribution on the electrolyte surface.

From both **Figs. 3a** and **b**, it is further obtained that the distribution of oxygen mole fraction on dense electrolyte has a similar configuration to that in rib channel region. The electrolyte surface covered by the rib channels will obtain a high value of oxygen mole fraction. The sites covered by the solid ribs, however, can only obtain very few oxygen moles fractions, because of the longer oxygen diffusing path and narrow transport cross section. Thus, the rib channel shape and geometric parameters are generally considered to be the important factors to affect the species distribution over the electrolyte surface.

Figs. 3a-f further show the distribution of oxygen mole fraction within the rib channels and over the dense electrolyte, while the width of the rib channels are changed from 2 mm to 3 and 4 mm. respectively. Comparing **Figs. 3a**, **3c** and **3e**, we can conclude that changing the widths of the rib channel has little effect on the oxygen mole fraction distribution within the air flow path, because the three stacks work under the same output electric current. Similar operating electric current means that both the fuel and oxygen consumption rates among the three stacks are similar, although different rib channel widths are adopted.

Comparing the **Figs. 3b**, **3d** and **3f**, however, we can find that increasing the rib channel width to a proper size will greatly improve the oxygen distribution quality over the dense electrolyte surface. The mole fraction value of oxygen over the electrolyte is greatly increased and the oxygen depletion area nearby the outlet also becomes smaller than the smaller rib channel width case. The reason is that larger rib channel width means bigger contact area between the rib channels and porous cathode and lower transporting resistance of oxygen diffusion.

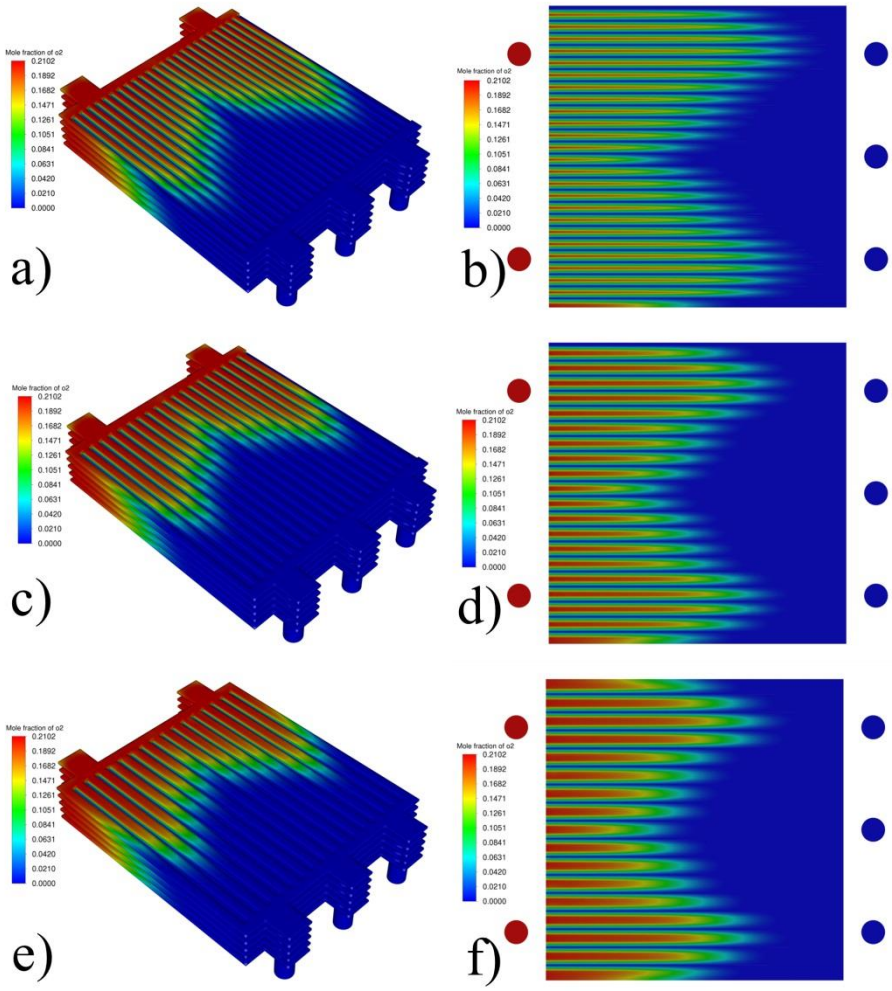

Figure 3. The oxygen distributions within the 5-cells PCFC stack and over the dense electrolyte surface for the widths of the rib channels equal to: a) 2 mm; c) 3 mm; e) 4 mm.

Similarly, **Figs. 4a-f** further show the vapor mole fraction distributions within the 5-cells PCFC stack and the dense electrolyte surfaces, while the width of the rib channels are changed from 2 mm to 3 and 4 mm. From **Fig. 4a** we can get the vapor distribution characteristics within rib channels is opposite to the oxygen mole fraction distribution in **Fig. 3a**. The vapor mole fraction will increase from the inlet manifold side to the outlet manifold side as long as oxygen is continuously consumed to produce vapor. The width of the rib channel determines the vapor removal capacity.

From **Figs. 4a**, **4c** and **4e**, we can get that there are similar vapor mole fraction distributions for the PCFC stack with three different rib channel widths, because of the same output electric current working conditions of the stacks. From **Figs. 4b**, **4d** and **4**f we can get that the vapor mole fraction distribution over the dense electrolyte surfaces will have the similar configuration with that within the rib channels zones. Obviously, the value of vapor mole fraction on electrolyte surface is different, due to vapor transfer resistance caused by the different contact area between the rib channel and porous cathode.

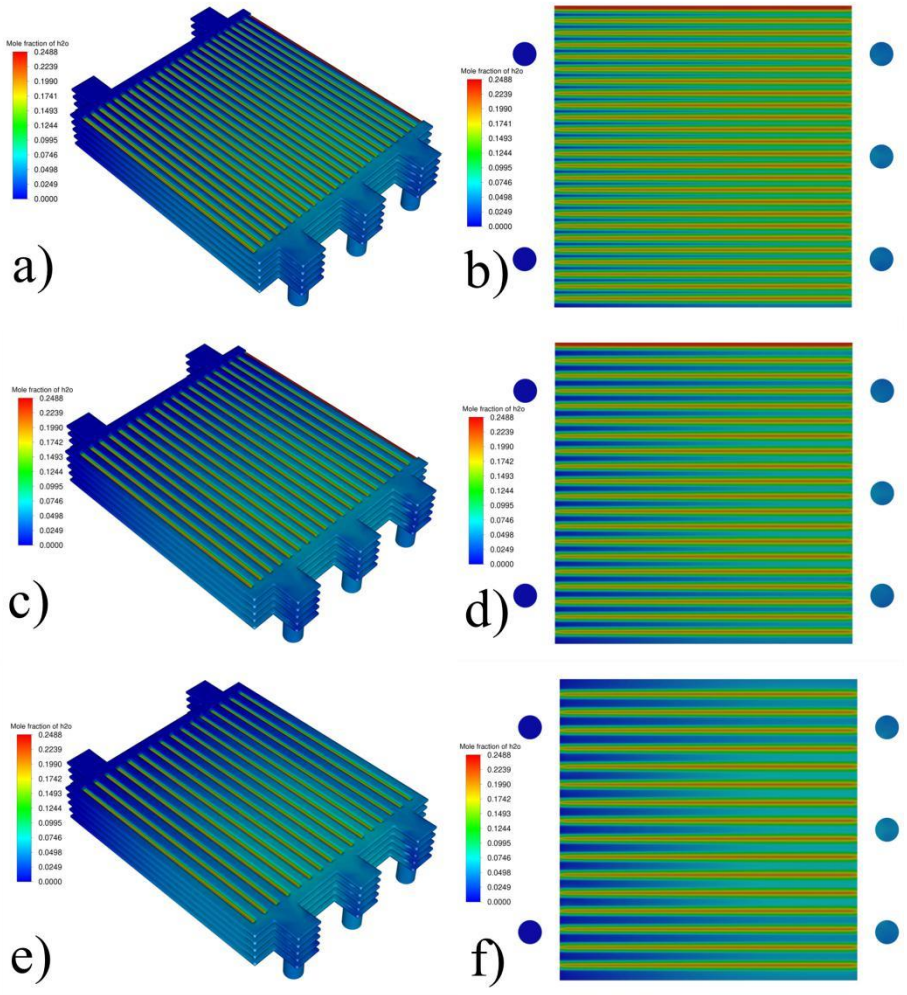

Figure 4. The vapor distributions within the 5-cells PCFC stack and over the dense electrolyte surface for the widths of the rib channels equal to: a) 2 mm; c) 3 mm; e) 4 mm.

Similarly, the distribution of nitrogen within the 5-cells PCFC stacks with different rib channels widths are shown in **Figs. 5a-c**, respectively.

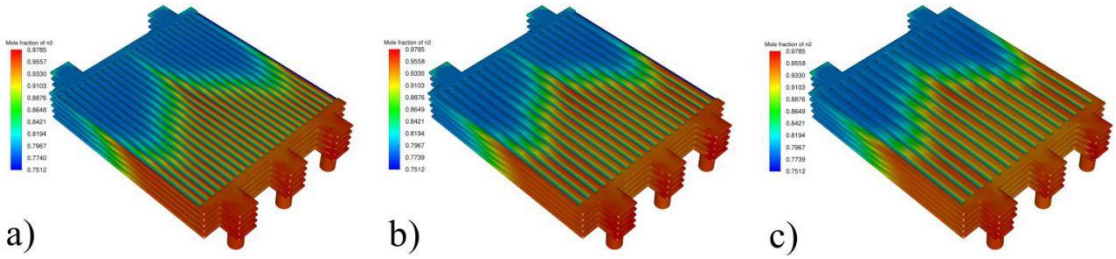

Figure 5. Distributions of the nitrogen within the 5-cells PCFC stacks with different rib channel widths: a) 2 mm; b) 3 mm; c) 4 mm.

In **Figs. 6** and **7,** the effects of various cathode thicknesses on the oxygen and vapor distribution over the dense electrolyte surface of PCFC stack are investigated. Increasing the cathode thickness of the PCFC can greatly improve the oxygen distribution qualities over the dense electrolyte surface and improve the electrochemical performance of the PCFC stack (shown in **Fig. 6**). It can also relief the transporting resistance of the produced vapor by the cathodic electrochemical reactions within PCFC cathode (shown in **Fig. 7**). Obviously, over thin porous PCFC cathode will lead to poor oxygen supply and vapor removal capacities. The enrichment of vapor in the cathode will accelerate the polarization phenomenon and degrade the performance of PCFC. Although increasing the thickness of the porous cathode will slightly increase the length of the species diffusing path, it will greatly enhance the cross section area of the diffusing path. This can greatly relief the transporting resistance caused by the solid ribs and increasing the oxygen supplying and vapor removing capabilities.

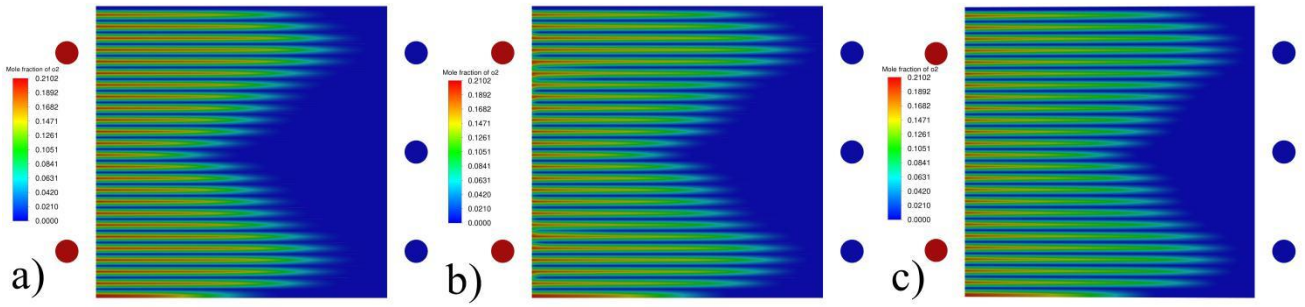

Figure 6. Dependence of the oxygen distribution over the cathode/electrolyte interface of 3-rd PCFC unit on the thickness of the porous PCFC cathode. a) 0.01 mm; b) 0.02 mm; c) 0.03 mm.

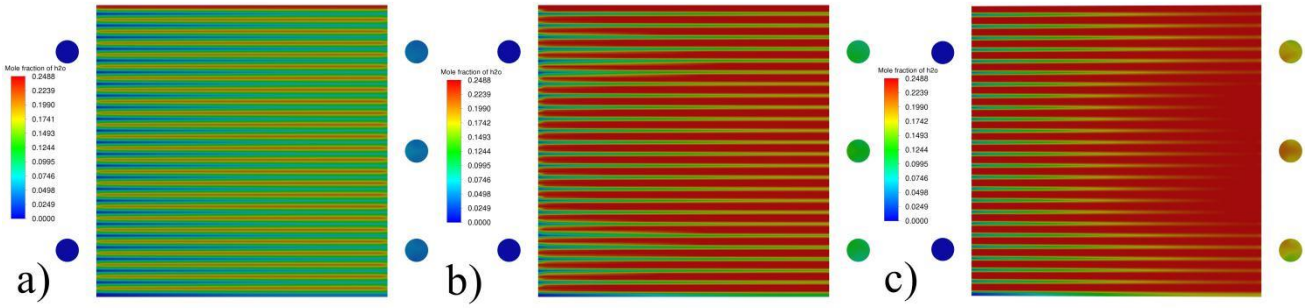

Figure 7. Dependence of the vapor distribution over the cathode/electrolyte interface of 3-rd PCFC unit on the thickness of the porous PCFC cathode: a) 0.01 mm; b) 0.02 mm; c) 0.03 mm.

The results of this paper can be compared with the oxygen distribution in previous studies on SOFC [25]. When the inlet and outlet directions are the same, the oxygen distribution in the cathode air flow channel is similar to that in this paper, and gradually decreases from the inlet direction to the outlet direction. Moreover, the distribution trends of oxygen over the electrolyte surfaces are also similar, which illustrates that under similar configurations, the distribution trends of oxygen in the cathode of

SOFC and PCFC are quite similar, except that PCFC will produce vapor in the cathode, which is a key factor to be considered when optimizing the cathode structure of PCFC.

4. CONCLUSION

In this paper, a three-dimensional model of 5-cells PCFC stack is established, and the effects of different geometric parameters and porous cathode thickness on oxygen transport and vapor removal are studied. Part of the following results are achieved.

i) The rib channel geometric parameters and inlet/outlet manifold positions are two important factors to determine the species distribution features within the rib channels and over the electrolyte surface.

ii) The sites covered by the solid ribs can only obtain very few oxygen moles fractions, because of the relative long oxygen diffusing path and narrow transport cross section.

iii) Increasing the thickness of the PCFC porous cathode can greatly enhance the cross-section area of the diffusing path and increasing the oxygen supplying and vapor removing capabilities for those electrolyte surface zone that covered by the solid ribs.

ACKNOWLEDGEMENTS

This research was funded by the financial support of the National natural science foundation of China (22179054), Ministry of science and technology of the People's Republic of China (CU03-10), Jiangsu province ‘333’ high level talents project and Department of education of Jiangsu Province.

References

1. Y. Zou, J. Li, J. Zhang, K. Ding, H. Wen. *Ionics,* 25 (2019) 4851.
2. B. Lin, Y. Shi, N. Cai. *Int. J. Hydrogen Energy*, 40 (2015) 3035.
3. W. Bi, J. Li, Z. Lin. *J. Power Sources*, 195 (2010) 3207.
4. K.J. Albrecht, A. Dubois, K. Ferguson, C. Duan, R.P. O’Hayre, R.J. Braun. *J. Electrochem. Soc.*, 166 (2019) F687.
5. Y. Xu, A. Kukolin, D. Chen, Wei. Yang. *Appl. Sci.,* 9 (2019) 1190.
6. C. Duan, J. Huang, N. Sullivan, R. O'Hayre. *Appl. Phys. Rev.,* 7 (2020) 011314 .
7. S. Zeng, X. Zhang, C.S. Jun, T. L, M. Andersson. *Int. J. Heat Mass Transfer*, 125 (2018) 506.
8. G. Yang, C. Su, H. Shi, Y. Zhu, Y. Song, W. Zhou, Z. Shao. *Energy & Fuels,* 34 (2020) 15169.
9. R. Strandbakke, V.A. Cherepanov, A.Y. Zuev, D.S. Tsvetkov, C. Argirusis, G. Sourkouni, S.Prünte, T. Norby. *Solid State Ionics,* 278 (2015) 120.
10. E. Anggia, E.-K. Shin, J.-T. Nam, J.-S. Park. *Ceram. Int.,* 46 (2020) 236.
11. D. Medvedev. *Int. J. Hydrogen Energy*, 44 (2019) 26711.
12. E.-K. Shin, E. Anggia, A.S. Parveen, J.-S. Park. *Int. J. Hydrogen Energy*, 44 (2019) 31323.
13. J.Q. Dai, M.F. Zhu, H.Z. Zhang, J.P. Liu, D.F. Chen. *Int. J. Electrochem. Sci.,* 16 (2021) 211052.
14. N. Wang, S. Hinokuma, T. Ina, C. Zhu, H. Habazaki, Y. Aoki. *J. Mater. Chem. A,* 8 (2020) 11043.
15. J. Zhao, Q. Jian, Z. Huang, L. Luo, B. Huang. *J. Power Sources,* 435 (2019) 226775.
16. S.H. Hwang, S.K. Kim, J.-T. Nam, J.-S. Park. *Int. J. Hydrogen Energy*, 46 (2021) 1076.
17. Z. Zhu, S. Wang. *Ceram. Int.,* 45 (2019) 19289.
18. Y. Okumura, Y. Nose, J. Katayama, T. Uda. *J. Electrochem. Soc.*, 158 (2011) B1067.

19. K. Li, T. Araki, T. Kawamura, A. Ota, Y. Okuyama. *Int. J. Hydrogen Energy,* 45 (2020) 34139.
20. S. Choi, C.J. Kucharczyk, Y. Liang, X. Zhang, I. Takeuchi, H.-I. Ji, S.M. Haile. *Nat. Energy*, 3 (2018) 202.
21. S. Su, S. Zhang, C. Yan, Z. Yang, F. Zheng, L. Zhang. *Int. J. Electrochem. Sci.,* 12 (2017) 230.
22. W. Bi, D. Chen, Z. Lin. *Int. J. Hydrogen Energy*, 34 (2009) 3873.
23. D. Chen, B. Hu, K. Ding, C. Yan, L. Lu. *Energies*, 11 (2018) 1875.
24. D. Chen, Y. Xu, B. Hu, C. Yan, L. Lu. *Energy Convers. Manage.*, 171 (2018) 807.
25. K. Ding, M. Zhu, Z. Han, V. Kochetov, L. Lu, D. Chen. *Ionics*, 26 (2020) 4567.
26. S. Maharudrayya, S. Jayanti, A.P. Deshpande. *J. Power Sources,* 157 (2006) 358.
27. T. Yuan, X. Wu, S.J. Bae, X. Zhu. *Reliab. Eng. Syst. Saf.*, 189 (2019) 157.
28. D. F. Chen, Z. Y. Chen, J. Li, J. Q. Zhang, K. Liu. *Int. J. Electrochem. Sci.*, 14 (2019) 2857.
29. C. Duan, J. Tong, M. Shang, S. Nikodemski, M. Sanders, S. Ricote, A. Almonsoori, R. O'Hayre, *Science*, 349 (2015) 1321.
30. D. Chen, H. Wang, S. Zhang, M.O. Tade, Z. Shao, H. Chen. *AlChE J.*, 61 (2015) 3786.
31. D. Chen, Y. Xu, M.O. Tade, Z. Shao. *ACS Energy Lett.*, 2 (2017) 319